Research Article Vol. 15, No. 12 / 1 Dec 2024 / Biomedical Optics Express 6756
Biomedical Optics EXPRESS

Tissue-probe contact assessment during robotic surgery using single-fiber reflectance spectroscopy

LOTTE M. DE ROODE,[1,2,*] LISANNE L. DE BOER,[1] HENRICUS J. C. M. STERENBORG,[1] AND THEO J. M. RUERS[1,2]

[1]*Image-Guided Surgery, Department of Surgery, the Netherlands Cancer Institute-Antoni van Leeuwenhoek, Plesmanlaan 121, Postbus 90203, 1066 CX Amsterdam, The Netherlands*
[2]*Department of Nanobiophysics, Faculty of Science and Technology, University of Twente, Drienerlolaan 5, 7522 NB Enschede, The Netherlands*
[*]*l.de.roode@nki.nl*

Abstract: The introduction of robotic surgery has improved minimally invasive surgery, and now robotic surgery is used in several areas of surgical oncology. Several optical techniques can be used to discriminate cancer from healthy tissue based on their optical properties. These technologies can also be employed with a small fiber-optic probe during minimally invasive surgery; however, for acquiring reliable measurements, some optical techniques require the fiber-optic probe to be in direct contact with the tissue. The lack of tactile feedback in robotic surgery makes assessing tissue-probe contact suitable for optical contact measurements challenging for the surgeon. In this study, we investigated the use of single fiber reflectance (SFR) to determine tissue-probe contact adequately. A machine learning-based algorithm was developed to classify if direct tissue-probe contact was present during the measurement in an ex-vivo tissue setup. Using this classification algorithm, an average accuracy of 93.9% was achieved for assessing probe-tissue contact, suggesting that this technique can be utilized to assess tissue-probe contact in an in vivo clinical setting.

1. Introduction

Surgical oncologists aim to remove malignant tumors while preserving healthy tissue and minimizing surgical trauma. Minimally invasive surgery, especially robotic surgery, offers several benefits to patients over open surgery, including shorter hospital stays, less pain, and reduced blood loss [1,2]. In surgical oncology, robotic surgery is now used in gynecologic, thoracic, endocrine, colorectal, hepato-pancreato-biliary, gastrointestinal, and urologic oncology. While urology and gynecology were early adopters of the technique, increased penetration of robotic surgery is seen in other areas of surgical oncology [3].

Although robotic surgery has many secondary advantages such as enhanced precision, dexterity, and control, allowing surgeons to perform more complex procedures with greater accuracy, reduced tremors, and improved visualization through 3D imaging, over open surgery, and other minimally invasive surgery, such as laparoscopic surgery, the oncologic outcome is equivalent [3]. This translates to PSM occurrence in up to 40% of oncological surgical procedures [4–8]. A positive surgical margin (PSM) indicates that tumor tissue was found at the resection margin, suggesting that the tumor may not have been completely removed. The impact of a PSM varies depending on the type of cancer surgery, but typically, it is linked to a poorer prognosis and the requirement for adjuvant treatments, which can be a further burden on both patients and the healthcare system [9].

Several optical techniques can be used for intraoperative margin assessment. Within our group, Diffuse Reflectance Spectroscopy has been researched for tumor detection in lung cancer surgery

#534558 https://doi.org/10.1364/BOE.534558
Journal © 2024 Received 3 Jul 2024; revised 18 Sep 2024; accepted 13 Oct 2024; published 11 Nov 2024

Biomedical Optics EXPRESS

(accuracy 91%), liver surgery (accuracy >90%), colorectal surgery (accuracy 92%), and breast cancer surgery (accuracy 95%) [10–14]. DRS is an optical technique that can differentiate tissue types based on their optical properties [15]. An important requirement for reliable DRS data is proper direct contact between the fiber-optic probe and the tissue. [15].The lack of tactile feedback in robotic surgery poses a challenge in assessing tissue-probe contact suitable for optical contact measurements for the surgeon [2]. When further researching the implementation of DRS in the clinical workflow, the need to assess tissue-probe contact suitable for optical contact measurements for surgeons during robotic surgery arose. The ability to accurately assess probe-tissue contact is not only valuable for DRS but also for other contact-requiring (optical) methods.

We propose using Single Fiber Reflectance (SFR) to quantify tissue-probe contact adequately. As the name suggests, SFR only requires one fiber through which light is emitted and received. The detected signal in SFR consists of 2 components: photons backscattered from inside the tissue and photons back-reflected from the fiber surface, where the latter is a relatively strong signal. Classical SFR, for tissue diagnostic purposes, focuses on the reflection from inside the tissue. Hence, it uses a fiber with a distal end polished under a 15-degree angle [16]. The angled tip strongly suppresses all internal reflections as they fall outside the Numerical Aperture (NA) of the fiber. In our approach, however, we will use a flat polished end generating a strong internal reflectance. By using flat polished fibers, the setup allows for SFR and DRS measurements to be acquired with one probe. It has no consequences for the DRS measurement, but for the SFR measurement, the internal reflection will be present, and its strength will depend on the refractive index of the fiber core and the medium directly in contact with its surface. According to the Fresnel equation for perpendicular incidence, see Eq. (1)

$$R = \left| \frac{n_1 - n_2}{n_1 + n_2} \right|^2 \tag{1}$$

in which R is the reflectance, n_1 is the refractive index of the fiber core, usually around 1.42, and n_2 is the refractive index of the medium in contact with the fiber tip. In the case of tissue, n_2 is in the range from 1.33-1.36; in the case of air, n_2 equals 1 [17]. This leads to approximate values for the internal reflection of 0.001 or less in the case of tissue contact and 0.03 in the case of air (i.e., no tissue contact).

We hypothesize that this difference in internal reflection is detectable and can be used to determine whether or not the probe makes contact with the tissue.

In addition, in a laparoscopic surgical environment, a situation might occur in which a droplet of water or blood is present between the probe and the tissue. During surgeries, it's possible for a drop of blood to stick to the probe because of the surface tension of the blood and the probe. If there's a lot of blood, the surgical cavity is flushed with water. If not all the water is removed, drops of water may stick to the probe due to the surface tension of the water and the probe. Since water (n = 1.33) and blood (n = 1.392) have refractive indices that are close to that of tissue, the reflectance might be less discriminative when there is a drop of blood or water between the probe and the tissue, compared to when there is air between the probe and the tissue; thus a measurement of a drop of blood or water might be interpreted as a contact measurement [17,18]. We hypothesize that the small difference in reflectance may still be possible to detect by a machine learning-based classification algorithm, able to distinguish whether tissue-probe contact suitable for optical contact measurements is obtained, i.e., no air, water, or blood between fiber and tissue.

The main objective of this study is to evaluate the effectiveness of SFR in determining proper contact between tissue and the probe in robotic procedures with limited tactile feedback. To investigate this, a phantom study was initially conducted to assess feasibility. This was followed by an ex vivo study in which SFR measurements were conducted on prostates, with or without

Biomedical Optics EXPRESS

a drop of blood or water between the probe and the prostate surface. An algorithm was then developed to classify tissue-probe contact using the SFR data collected ex vivo.

2. Materials and methods

2.1. Spectroscopy setup

For this experiment, a combined DRS/SFR probe was designed to suit laparoscopic/robotic procedures. The probe has two fibers with a fiber-to-fiber distance of 2 mm; one fiber functioned as a receiving fiber for DRS measurements (for acquiring tissue optical properties), and the other fiber served as an emitting fiber for DRS measurements and as both a receiving and emitting fiber for SFR. The probe was connected to a spectroscopy system comprising the following components;

- Two halogen broadband light sources (Avantes, AvaLight-HAL) covering the wavelength range from 360 to 2500 nm, which possess a USB controllable shutter.
- Two spectrometers. One spectrometer operated in the visible wavelength range from 200 to 1160 nm (Avantes, AVASPEC-HS2048XL-EVO), while the other covered the near-infrared range from 900 to 1750 nm (Avantes, AVASPECNIR256-1.7-RS).
- A single 100-micron patch cable and a trifurcated 3x100-micrometer fiber cable (having 3 separate 100-micron fiber connectors on one side and a single fiber connector on the other side combining the 3 100-micron fibers into one connector).
- A fiberoptic measurement probe consisting of two 400 micron fibers exiting the probe at the distal end with a 2 mm distance.

Figure 1 presents an overview of the spectroscopy system and probe. The control of these components and data processing were accomplished using custom MATLAB software developed in-house. While the setup allowed for combined DRS/SFR measurements, only the SFR measurements were used for this study.

2.1.1. Data acquisition

Before starting the measurement procedure, the system was calibrated to ensure accurate reflectance readings by correcting for environmental factors and equipment variability [19]. The calibration procedure for the combined SFR and DRS probe involves three key reference measurements: a measurement on Spectralon (Avantes WS-2, Avantes, Apeldoorn, The Netherlands) for spectral sensitivity, I_{white}, a measurement in water for internal reflection correction, I_{water}, and a dark measurement, I_{dark}, to account for ambient noise. The dark measurements were performed with all light sources switched off just before each measurement to compensate for the possible influence of (variable) ambient light. The entire calibration procedure was performed with the ambient lights switched off. The SFR reflection of a sample R_{cal} is then calculated from a measurement I_{meas}, see Eq. (2).

$$R_{cal} = \frac{(I_{meas} - I_{dark}) - (I_{water} - I_{dark})}{(I_{white} - I_{dark}) - (I_{water} - I_{dark})} \tag{2}$$

After the calibration measurements were acquired, the system was ready to start the measurement procedure. Each measurement procedure was performed with the ambient light switched off. Each measurement within the measurement procedure consisted of three cycles of a DRS measurement followed by an SFR measurement. For a DRS measurement, Lamp 1 was switched on; light was sent through Fiber 1 into the tissue, collected from the tissue, and sent to the two spectrometers by Fiber 2. For an SFR measurement, Lamp 2 was switched on; the light was sent

Biomedical Optics EXPRESS

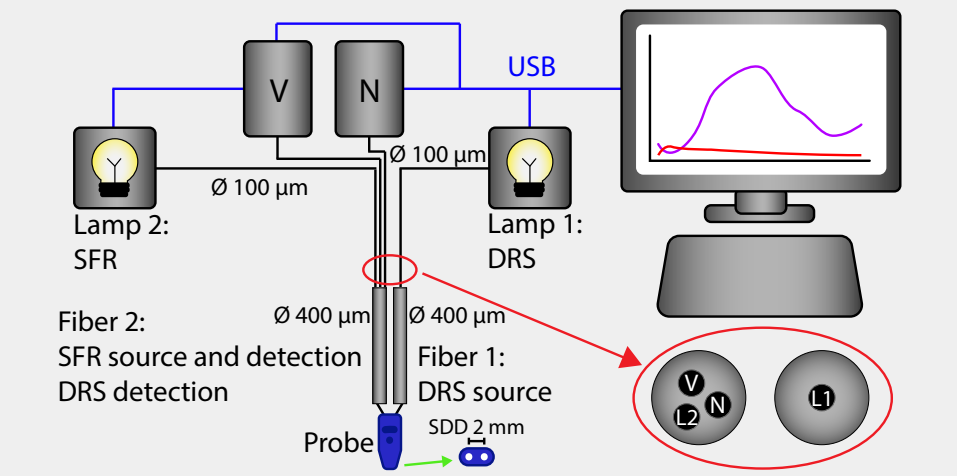

Fig. 1. Overview of measurement setup. Two halogen light sources are used (Lamp 1 and Lamp 2) and two spectrometers (V, visible wavelength range, N, near-infrared wavelength range). For a DRS measurement, Lamp 1 is switched on. It is connected to Fiber 1 of the probe via a 100-micron fiber and leads the light to the tissue. At a 2 mm distance from Fiber 1, Fiber 2 collects light from the tissue and leads the light via two 100-micron fibers of the trifurcated fiber to the two spectrometers. For an SFR measurement, Lamp 2 is switched on. It is connected to Fiber 2 of the probe via the third 100-micron fiber of the trifurcated fiber. Again, Fiber 2 collects light from the tissue as well as the internal reflection and leads it to the spectrometers. The red-circled enlarged inset shows the connection between the 100-micron and 400-micron fibers. It uses two standard SMA fiberoptic connectors, connecting the 400-micron Fiber 1 to the 100-micron Lamp 1 fiber and the 400-micron Fiber 2 to the three sets of 100-micron fibers to Lamp 2 and the two spectrometers. This construction functions as a beam splitter with a very low (light source-to-detector) crosstalk. The green arrow points towards a schematic of the probe surface.

through Fiber 2 into the tissue, collected from the tissue, and sent to the two spectrometers by the same Fiber 2. Per measurement, the reflectance values for each wavelength over the three cycles were averaged to calculate one reflectance value for each wavelength per DRS and per SFR measurement. For this research, only the collected SFR reflectance values were stored.

2.2. Measurement procedure

2.2.1. Phantom study

A solid phantom was created for the phantom experiment by water-dissolved agarose as the base material (Sigma-Aldrich, 0.84% concentration) and Intralipid as the scattering material (Intralipid-20% solution, dilution 1/20) while Evans blue (Proveblue 5mg/mL, 0.28% concentration) was added as an absorbing agent, which strongly absorbs light around a wavelength of 608 nm. After mixing the agarose, Intralipid, and Evans blue, the liquid phantom was put into the fridge to solidify. One phantom (70 mm x 56 mm) was used for the phantom study. The phantom was placed on a flat surface, and the calibrated probe was fixed in a static holder that allowed precise adjustment of the probe-to-tissue distance, see Fig. 2.

First, the probe was placed in contact with the phantom, and three consecutive measurements were obtained. Subsequently, the probe-to-phantom distance was increased incrementally with steps of 0.5 mm to a maximum of 2.0 mm distance between the probe and the phantom. At each step, a measurement was conducted. Second, because droplets of water might adhere to the probe tip in an in vivo situation, the probe was again placed in contact with the phantom for

Biomedical Optics EXPRESS

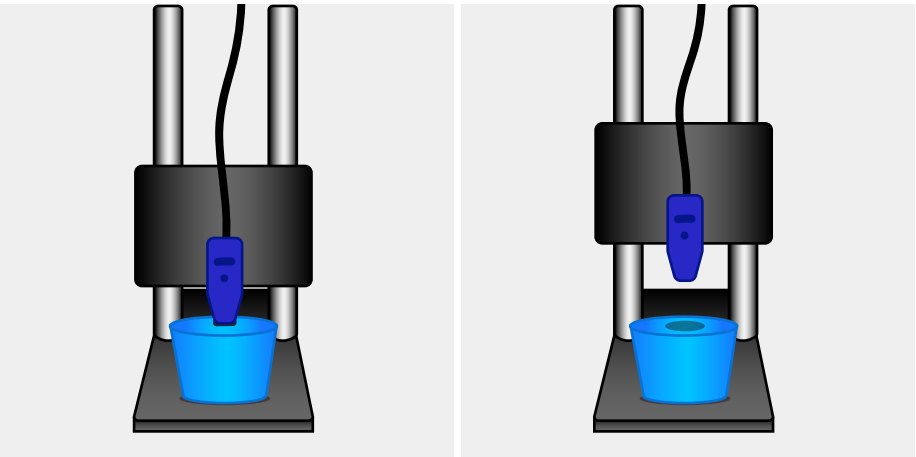

Fig. 2. Measurement setup with phantom lying on a flat surface and probe in the static holder. The left side of the figure shows phantom-probe contact and the right side of the figure shows no phantom-probe contact.

water measurements. This time, a syringe was used to put a drop of water between the probe and the phantom prior to each measurement. The probe-to-phantom distance was again increased incrementally with steps of 0.5 mm. At each step, a measurement was conducted with a drop of water between the probe and the phantom. When the distance between the phantom and the probe is shorter, it means that the liquid is in contact with both the probe and the phantom. When the distance is increased, the liquid sticks to the probe.

2.2.2. Ex vivo tissue study

This ex vivo study was performed in compliance with the Declaration of Helsinki and approved by the Institutional Review Board of The Netherlands Cancer Institute/Antoni van Leeuwenhoek (Amsterdam, the Netherlands). According to Dutch law (WMO), no written informed consent from patients was required. Five prostate specimens were included in the ex vivo tissue study. Prostates were collected from the operating room after prostate cancer surgery. Each prostate was placed on a flat surface, and the calibrated probe was fixed in a static holder that allowed precise adjustment of the probe to tissue distance, see Fig. 3. Firstly, the probe was brought into contact with the prostate tissue, and a measurement was taken. Then, the probe was lifted 0.5 mm, and a new measurement was taken. This process was repeated until the probe had been lifted 7.5 mm. The distance between the prostate and the probe was increased incrementally to ensure that measurements without contact were obtained. Because the prostate is a pliable organ, tissue contact could still be present even after increasing the distance by one increment. After each increment, the researcher assessed whether the probe made adequate tissue contact. Finally, this process was repeated in the opposite direction, thus lowering the probe, resulting in a total of 32 measurements.

Because in an in vivo situation, droplets of water or blood may adhere to the probe tip, this experiment was repeated with the probe tip immersed in water and blood. When the distance between the prostate and the probe is shorter, it means that the liquid is in contact with both the probe and the prostate. When the distance is increased, the liquid (whether water or blood) sticks to the probe. Again, the researcher visually assessed whether the probe made tissue contact and noted whether the probe had lost adequate contact.

For this experiment, only the SFR measurements for tissue contact assessment were of importance, and thus, the DRS results were disregarded.

Biomedical Optics EXPRESS

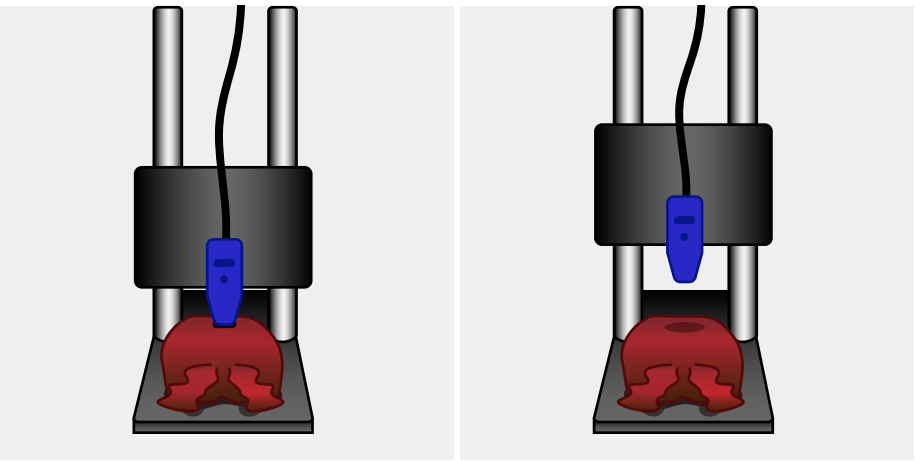

Fig. 3. Measurement setup with prostate lying on a flat surface and probe in the static holder. The left side of the figure shows tissue-probe contact, and the right side of the figure shows no tissue-probe contact.

2.3. Data analysis

A classification model was trained to predict tissue-probe contact. The input data comprised the acquired broad-band SFR spectra, while the output labels for training the model were determined based on the researcher's visual assessment of tissue-probe contact. To reduce the number of features and thus prevent overfitting, features were calculated based on 1) the average reflectance over all wavelengths, 2) a wavelength range from 400 to 1000 um, 3) a wavelength range from 1000 um to 1600 um, and 4) a wavelength range from 700 to 1300 um, resulting in a total of four features. These four features were used as input data. The output labels were labeled as either "Contact," "No Contact Dry," or "No Contact Water or Blood". If the probe had contact through a droplet of water or blood for the blood and water measurements, it was labeled as "No Contact Water or Blood". The data was split into a train set (70%) and a test set (30%). The model used a Support Vector Machine (SVM) with a linear kernel and was trained through a 10-fold cross-validation technique to classify tissue-probe contact. The choice of an SVM model with a linear kernel was made due to its simplicity, which ensures that the model remains interpretable and less prone to overfitting. Additionally, the computational efficiency of SVM, especially with a linear kernel, allows for a quick and accurate classification without the need for extensive computational resources. This enables easy integration into a real-time surgical environment. The performance of the model was evaluated by the accuracy, area under the curve (AUC), Matthews Correlation Coefficient (MCC), sensitivity, and specificity over ten iterations of the test set. Thus, the original dataset was divided into a 70% train set and a 30% test set ten times, ensuring different combinations of train data and test data in each iteration to increase generalizability. For clinical application, it is important to know whether there is proper tissue-probe contact suitable for optical measurements. It is irrelevant to know if either blood or water is present at the tip if there is no proper contact. Therefore, the performance was evaluated on two output labels: "Contact" and "No Contact," merging the outcomes from "No Contact Dry" and "No Contact Water or Blood" into a single class "No Contact".

Biomedical Optics EXPRESS

3. Results

3.1. Phantom study

A total of eleven measurements were included in this phantom study, of which three were with the probe in contact with the phantom, four were with air between the probe and the phantom, and four were with water between the probe and the phantom. Figure 4 shows the average spectra and standard deviation for contact measurements, measurements with air between the probe and the phantom, and measurements with water between the probe and the phantom.

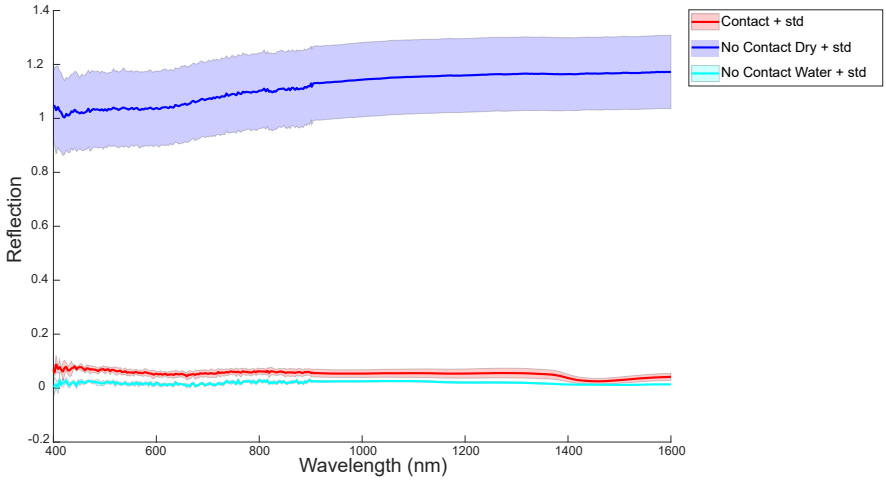

Fig. 4. Single Fiber Reflectance (SFR) mean spectra and standard deviation (std) for No Contact measurements (with air between the probe and the phantom) in dark blue, for No Contact Water measurements (with water between the probe and the phantom) in cyan, and for Contact measurements in red on the phantom experiments

The difference in reflectance between contact measurements and measurements with air between the probe and the phantom (no contact) was much more evident than the difference in reflectance between contact measurements with water between the probe and the phantom (no contact). Nevertheless, there was no overlap in reflectance. The average reflectance value for contact measurements in this phantom experiment was 0.05 (std 0.02); for measurements with air between the probe and the phantom, it was 1.12 (std 0.13); and for measurements with water between the probe and the phantom, it was 0.02 (std 0.01). As expected, the internal refraction measured with air between the probe and the phantom was more than ten times as high as the internal refraction measured in the contact measurements. The difference between air and water was much smaller.

3.2. Ex vivo tissue study

3.2.1. Dataset

A total of five prostates were included in this ex vivo tissue study, leading to a total of 466 measurements, of which 156 were without water or blood, 155 with blood, and 155 with water. Table 1 provides an overview of all measurements.

3.2.2. Classification

On dry prostates, the SFR spectra from Contact measurements have a much lower intensity compared to the SFR spectra from No Contact measurements. Figure 5 shows the SFR spectra of Contact and No Contact measurements for dry prostates, as well as for the water and blood

Biomedical Optics EXPRESS

Table 1. Number of measurements

	Contact	No Contact
Dry	43	113
Water	44	111
Blood	42	113

measurements. The difference between Contact measurements (red) and Dry No Contact measurements (dark blue) is very clear. The SFR spectra from Contact measurements (red) and No Contact Water (cyan) or No Contact Blood (magenta) are more overlapping, and it is not possible to clearly distinguish them visually.

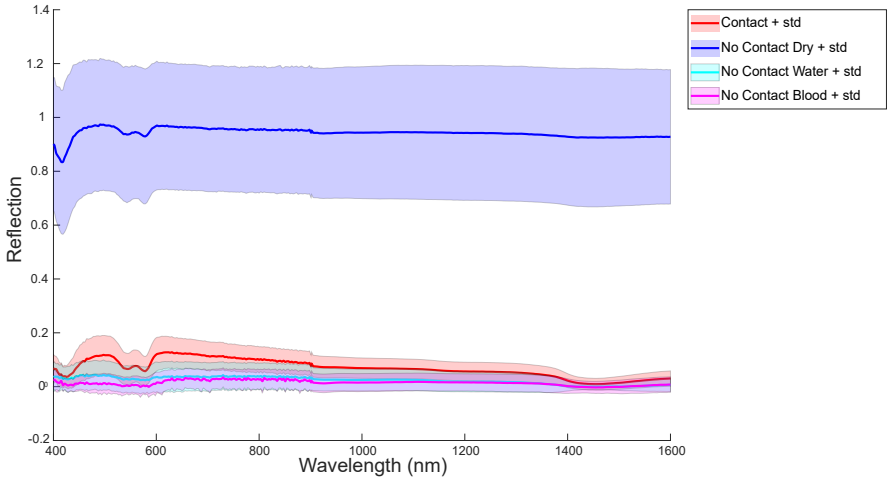

Fig. 5. Single Fiber Reflectance (SFR) mean spectra and standard deviation (std) for No Contact Dry measurements (dark blue), No Contact Water measurements (cyan), No Contact Blood measurements (magenta) and Contact measurements (red).

The average reflectance values and their standard deviations for the four features for Contact measurements, for No Contact Dry measurements, and for No Contact measurements in the presence of water and blood are shown in Table 2. Again, there is no overlap in the average reflectance values for Contact measurements and No Contact Dry measurements, but the difference between Contact measurements and No Contact Water or Blood Measurements is much smaller with some slight overlap in standard deviations.

Table 2. Average reflectance values and their standard deviations for the four features for Contact measurements, for No Contact measurements on dry prostate and for No Contact measurements on prostates in the presence of water or blood.

	All wavelenghts		400 - 1000 nm		700 - 1300 nm		1000 - 1600 nm	
	Average	Std	Average	Std	Average	Std	Average	Std
Contact	0.07	0.04	0.09	0.05	0.08	0.04	0.04	0.03
No Contact Dry	0.94	0.24	0.95	0.24	0.95	0.24	0.94	0.25
No Contact Water or Blood	0.02	0.04	0.03	0.04	0.02	0.04	0.01	0.03

After training the model using the four features and applying the model to the test set on ten different combinations of training and testing data, the model was able to classify the acquired SFR data in the unseen test set with an average accuracy of 93.9%, an average sensitivity of

Biomedical Optics EXPRESS

92.2%, an average specificity of 94.7%, an average MCC of 0.85, and an average AUC of 0.95. Table 3 presents an overview of these metrics and their standard deviation. All misclassified spectra were of measurements with water or blood, as can be seen in the confusion matrix depicted in (Fig. 6).

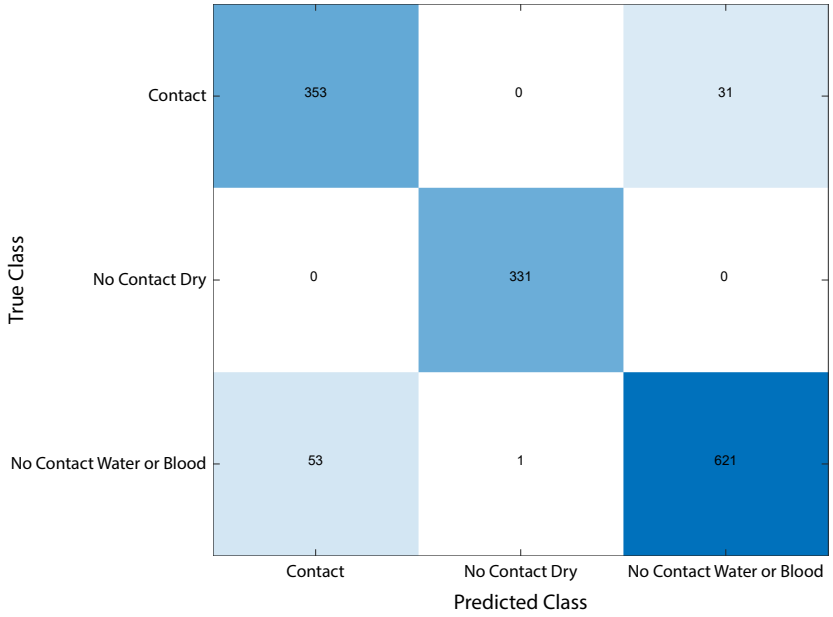

Fig. 6. Confusion matrix showing the sum of the results from ten different iterations. "Contact" adheres to measurements in which the probe made contact with the tissue, regardless of the presence of water or blood. "No Contact Dry" adheres to measurements in which the probe did not make contact with the tissue without the presence of water or blood. "No Contact Water or Blood" adheres to measurements in which the probe did not contact the tissue and water or blood was present. All misclassified spectra were from Blood or Water measurements.

Table 3. Average and standard deviation (std) from precision, sensitivity, specificity, accuracy, Matthews Correlation Coefficient (MCC), and Area Under the Curve (AUC) out of ten different test runs

Sensitivity		Specificity		Accuracy		MCC		AUC	
Average	Std	Average	Std	Average	Std	Average	Std	Average	Std
92.2%	4.6%	94.7%	3.0%	93.9%	1.5%	0.85	0.04	0.95	0.01

When looking at the misclassified labels, we found that 8.06% of measurements with no probe-tissue contact and water or blood between the probe and the tissue were mislabeled as measurements with probe-tissue contact and that 8.57% of measurements with probe-tissue contact were mislabeled as measurements with no probe-tissue contact and water or blood between the probe and the tissue (Fig. 6).

4. Discussion

The aim of this study was to explore the feasibility of using SFR to detect contact between tissue and a fiberoptic probe. This could be particularly useful in situations with limited tactile feedback, such as in robotic surgery, as it would enable the assessment of tissue composition at

Biomedical Optics EXPRESS

the resection plane using contact requiring fiberoptic techniques, such as DRS. We conducted experiments using a phantom to confirm the feasibility of using SFR to determine probe contact. We then collected a dataset of SFR spectra that included measurements of where there was contact between the probe and freshly excised prostate tissue and where there was no contact. We also included spectra of measurements where the probe and prostate were wet due to the presence of water or blood, simulating conditions that may occur in a surgical setting. Finally, we developed a machine learning model to differentiate between probe-tissue contact and no probe-tissue contact accurately.

A phantom experiment was conducted to determine if SFR could be used to confirm probe contact. The experiment showed that when the phantom and the probe were dry, the average intensity of the SFR signal from probe-phantom contact measurements was much lower than the average intensity of the SFR signal from no probe-phantom contact measurements (Fig. 4). Even when the phantom or the probe was wet, the average intensity of the SFR signal over all wavelengths from probe-phantom contact measurements (0.053 (std 0.016)) did not overlap with the average intensity of the SFR signal over all wavelengths from no probe-phantom contact measurements (0.019 (std 0.006)), although the difference was smaller compared to the difference in average intensity over all wavelengths between contact measurements and no contact measurements when the phantom and the probe were dry. These results strengthen the idea that SFR can differentiate between probe contact and no probe contact.

An ex vivo tissue experiment was performed to further confirm the feasibility of SFR in determining probe-tissue contact. In this experiment, we aimed to simulate a situation in which a drop of water or blood would stick to the probe. This situation can occur in a clinical or surgical setting, for example, if there is a temperature difference between the abdomen and the probe, causing condensation and resulting in waterdrops sticking to the probe. Another instance where a drop of blood or water may adhere to the probe is when there is bleeding and the abdomen has been flushed with saline to restore camera vision. For this ex vivo tissue study, an experiment setup similar to the phantom experiment was used, but now, not only the influence of water on the SFR signal but also the influence of blood on the SFR signal was investigated. The mean spectra per contact type (either probe-tissue contact, or no probe-tissue contact with a dry probe and prostate, or no probe-tissue contact with water between the probe and prostate, or no probe-tissue contact with blood between the probe and prostate) were calculated, and shown in Fig. 5. Similar to the phantom measurements, there is a clear difference in intensity between probe-tissue contact measurements and no probe-tissue contact measurements on a dry prostate. The difference in intensity between probe-tissue contact and no probe-tissue contact measurements on prostates with water or blood between the probe and the tissue is much smaller and cannot be determined visually. However, by training a linear SVM model using the average intensity over all wavelengths, the average intensity over the first 600 wavelengths, the average intensity over the middle 600 wavelengths, and the average intensity over the final 600 wavelengths as input probe-tissue contact could be classified (Table 3). A linear Support Vector Machine (SVM) identifies the best hyperplane that maximizes the margin between two classes (in this scenario, Contact vs. No Contact). Despite some classes appearing clustered in certain plots in this dataset, the linear SVM effectively separated the two groups in the four-dimensional space provided by the selected features. The SVM's decision boundary effectively distinguished between tissue-probe contact and no-contact situations, as indicated by the high model performance.

As depicted in Table 1, the dataset was quite unbalanced, with more non-contact measurements than contact measurements. Therefore, we chose to use the Matthews Correlation Coefficient (MCC) as an evaluation metric, as it provides a holistic measure of model performance by considering all elements of the confusion matrix, effectively addressing class imbalance. Additionally, by relying on MCC, we maintained a more straightforward and more computationally efficient approach without introducing the complexity of modifying the dataset. These results

Biomedical Optics EXPRESS

suggest that SFR can accurately differentiate between probe-tissue contact and no probe-tissue contact, even in situations where drops of water or blood are present between the probe and the tissue.

This study is the first to investigate the use of SFR for detecting probe-tissue contact. It is important to note that classical SFR, for tissue diagnostic purposes, uses a fiber with a distal end polished under a 15-degree angle in order to suppress internal refraction [16,20]. This is preferable because the internal reflection is at least as large but usually much larger than the backscattered light from inside the tissue. Removing the internal reflection then significantly increases the signal-to-noise ratio of a measurement. In the current study, as our focus was on the internal reflection, we used a flat polished fiber, thus using the internal reflection to determine tissue contact instead of eliminating it. It is important to note that for the clinical application of this system, we are not interested in using SFR to measure tissue composition. In this manuscript, we wanted to investigate if SFR can be used to assess tissue-probe contact that is suitable for optical measurements of tissue. The strong point of using this combined SFR and DRS setup is that no additional sensors or fibers must be added to the measurement probe, as the existing flat-tipped fibers for DRS could be utilized for the SFR measurements. Thus, utilizing a simple and elegant design. A comparable design can be utilized for other fiber-optic probes where tissue-probe contact is necessary. Other studies focused on using sensors to mimic tactile feedback in robotic surgery settings and thus enable some form of palpation during robotic surgery [21,22]. While these sensors provided some tactile feedback to the surgeon, the problem they were trying to solve was much more complex than just the tissue-probe contact assessment, and the techniques were much more complicated.

To acknowledge the limitations of this study and highlight areas for future research, we note two key constraints. First, the relatively small and unbalanced dataset, though partly addressed by employing the MCC as an evaluation metric, presents limitations in the generalizability of the findings. Second, the results are based solely on ex vivo experiments. Although the results are based solely on ex vivo experiments, we sought to mimic in vivo conditions by testing the model's performance in the presence of water and blood, which partly mitigates this limitation. However, future research should still focus on in vivo implementations to fully validate the model's effectiveness in situations with limited tactile feedback, such as in robotic surgery.

5. Conclusion

In this study, the feasibility of using SFR for detecting probe-tissue contact during robotic surgery was examined. In an ex vivo study that simulated a clinical surgical setting, a linear SVM model could classify probe-tissue contact on an unseen test set with an average accuracy of 93.9%. These results suggest that SFR can be used for detecting probe-tissue contact for DRS measurements, as well as other contact-requiring optical methods utilizing a fiber-optic probe, during robotic surgery and thus allow for further research into the applications of DRS for surgical margin management.

Funding. Research at the Netherlands Cancer Institute; Dutch Cancer Society and of the Dutch Ministry of Health, Welfare and Sport.

Acknowledgments. The authors thank all urologists and nurses from the Department of Surgery at the Netherlands Cancer Institute for their assistance in collecting prostate specimens.

Disclosures. The authors declare no conflicts of interest.

Data availability. Data underlying the results presented in this paper are not publicly available at this time but may be obtained from the authors upon reasonable request.

References

1. J. Chang and D. W. Rattner, "History of minimally invasive surgical oncology," Surg. Oncol. Clin. North Am. **28**(1), 1–9 (2019).

Biomedical Optics EXPRESS

2. D. M. Herron and M. Marohn, and The SAGES-MIRA Robotic Surgery Consensus Group, "A consensus document on robotic surgery," Surg. Endosc. **22**(2), 313–325 (2008).
3. S. B. Hays, G. Corvino, B. D. Lorié, *et al.*, "Prince and princesses: the current status of robotic surgery in surgical oncology," J. Surg. Oncol. **129**(1), 164–182 (2024).
4. O. Yossepowitch, A. Briganti, J. A. Eastham, *et al.*, "Positive surgical margins after radical prostatectomy: a systematic review and contemporary update," Eur. Urol. **65**(2), 303–313 (2014).
5. R. A. M. Hassan, J. Y. Maesaka, M. D. Ricci, *et al.*, "Predictive factors for positive surgical margins in the treatment of breast ductal carcinoma in situ," J. Cancer Res. Ther. **12**(2), 995 (2016).
6. J. R. Bundred, S. Michael, B. Stuart, *et al.*, "Margin status and survival outcomes after breast cancer conservation surgery: prospectively registered systematic review and meta-analysis," The BMJ **378**, e070346 (2022).
7. A. Nießen, M. Loos, K. Neumüller, *et al.*, "Impact of circumferential resection margin on survival in ampullary cancer: retrospective analysis," BJS Open **7**(6), zrad120 (2023).
8. N. Pencovich, R. Houli, N. Lubezky, *et al.*, "R1 resection of colorectal liver metastasis – What is the cost of marginal resection?" J. Surg. Oncol. **119**(3), 347–354 (2019).
9. R. K. Orosco, V. J. Tapia, J. A. Califano, *et al.*, "Positive surgical margins in the 10 most common solid cancers," Sci. Rep. **8**(1), 5686 (2018).
10. J. W. Spliethoff, L. L. de Boer, M. A. J. Meier, *et al.*, "Spectral sensing for tissue diagnosis during lung biopsy procedures: The importance of an adequate internal reference and real-time feedback," Lung Cancer **98**, 62–68 (2016).
11. J. W. Spliethoff, L. L. de Boer, M. A. J. Meier, *et al.*, "In vivo characterization of colorectal metastases in human liver using diffuse reflectance spectroscopy: toward guidance in oncological procedures," J. Biomed. Opt. **21**(9), 097004 (2016).
12. F. Geldof, M. Witteveen, H. J. C. M. Sterenborg, *et al.*, "Diffuse reflection spectroscopy at the fingertip: design and performance of a compact side-firing probe for tissue discrimination during colorectal cancer surgery," Biomed. Opt. Express **14**(1), 128–147 (2023).
13. D. Veluponnar, B. Dashtbozorg, L.-J. S. Jong, *et al.*, "Diffuse reflectance spectroscopy for accurate margin assessment in breast-conserving surgeries: importance of an optimal number of fibers," Biomed. Opt. Express **14**(8), 4017 (2023).
14. L. L. de Boer, E. Kho, K. K. Van de Vijver, *et al.*, "Optical tissue measurements of invasive carcinoma and ductal carcinoma in situ for surgical guidance," Breast Cancer Res. **23**(1), 59 (2021).
15. S. L. Jacques and B. W. Pogue, "Tutorial on diffuse light transport," J. Biomed. Opt. **13**(4), 041302 (2008).
16. S. C. Kanick, C. van der Leest, J. G. J. V. Aerts, *et al.*, "Integration of single-fiber reflectance spectroscopy into ultrasound-guided endoscopic lung cancer staging of mediastinal lymph nodes," J. Biomed. Opt. **15**(1), 017004 (2010).
17. R. Khan, B. Gul, S. Khan, *et al.*, "Refractive index of biological tissues: Review, measurement techniques, and applications," Photodiagn. Photodyn. Ther. **33**, 102192 (2021).
18. D. J. Faber, M. C. G. Aalders, E. G. Mik, *et al.*, "Oxygen saturation-dependent absorption and scattering of blood," Phys. Rev. Lett. **93**(2), 028102 (2004).
19. X. U. Zhang, A. L. Post, D. J. Faber, *et al.*, "Single fiber reflectance spectroscopy calibration," J. Biomed. Opt. **22**(10), 1 (2017).
20. A. L. Post, A. J. de Groof, X. U. Zhang, *et al.*, "Toward improved endoscopic surveillance with multidiameter single fiber reflectance spectroscopy in patients with Barrett's esophagus," J. Biophotonics **14**(4), e202000351 (2021).
21. A. Abiri, Y.-Y. Juo, A. Tao, *et al.*, "Artificial palpation in robotic surgery using haptic feedback," Surg. Endosc. **33**(4), 1252–1259 (2019).
22. Q. Ouyang, J. Wu, S. Sun, *et al.*, "Bio-inspired haptic feedback for artificial palpation in robotic surgery," IEEE Trans. Biomed. Eng. **68**(10), 3184–3193 (2021).